Journal of *Respiration*

MDPI

Article

Exploring New Therapeutic Targets in NSCLC: Unraveling the Interplay Between NTRK and PD-L1 Expression

Jair Gutierrez-Herrera [1], Maria Angeles Montero-Fernandez [2], Georgia Kokaraki [3], Luigi De Petris [4,5], Raul Maia Falcão [6], Ricardo Guijarro [7], Simon Ekman [4,5] and Cristian Ortiz-Villalón [1,4,*]

1 Department of Clinical Pathology and Cancer Diagnostics, Karolinska University Hospital, F46, 14186 Stockholm, Sweden; jairmgh@gmail.com
2 Department of Cellular Pathology, Liverpool Clinical Laboratories, Clinical Support Services Building (CSSB), Royal Liverpool University NHS Foundation Trust, Mount Vernon Street, Liverpool L7 8YE, UK; amonterofer@hotmail.com
3 Center for Disease Neurogenomics, Icahn School of Medicine Mount Sinai, New York, NY 10029, USA; gkokaraki@gmail.com
4 Department of Oncology-Pathology (Onkpat), Karolinska Institute, 14186 Stockholm, Sweden; luigi.depetris@ki.se (L.D.P.); simon.ekman@ki.se (S.E.)
5 Thoracic Oncology Center, Theme Cancer, Karolinska University Hospital, 14186 Stockholm, Sweden
6 Genetics Department, Federal University of Pernambuco, Recife 50670-901, Brazil; raulmfalcao@gmail.com
7 Department of Surgery, Valencia University, 46010 Valencia, Spain; guijarro_ricjor@gva.es
* Correspondence: cristian.ortiz-villalon@ki.se; Tel.: +46-728751551

Abstract

Background: Precision medicine has introduced immune checkpoint inhibitors (ICIs) and tyrosine kinase inhibitors (TKIs) as key therapies for lung cancer. However, the interaction between PD-L1 expression and *NTRK* rearrangements in non-small cell lung cancer (NSCLC) remains unclear. **Methods:** A cohort of 482 resected NSCLC cases was analyzed using tissue microarrays. Immunohistochemistry (IHC) assessed PD-L1 expression with four antibody clones and pan-TRK with one clone. Whole-exome sequencing (WES) identified *NTRK* mutations, copy number variations, and gene fusions. Associations with clinicopathological features and prognosis were evaluated using Cox regression and survival analyses. Potential molecular connections between NTRK and PD-L1 were explored through a multi-database interactome analysis using Cytoscape. **Results:** PD-L1 positivity (TPS $\geq$ 1%) varied by clone: 28-8 (41.5%), 22C3 (34.2%), SP263 (42.7%), and SP142 (10.4%). High PD-L1 expression (TPS $\geq$ 50%) correlated with poorer overall survival in SP142-assessed cases ($p = 0.045$). TRK expression was observed in 4.6% (22/482) of cases, predominantly in squamous cell carcinoma (72.7%). Co-expression of pan-TRK and PD-L1 was significant ($p < 0.001$), with 4.6% of tumors showing dual positivity. WES detected three *NTRK* rearrangements, with no direct association with survival. **Conclusions:** The co-expression of PD-L1 and pan-TRK observed in this cohort suggests a biologically relevant interaction that warrants further investigation into its potential role in treatment response and resistance mechanisms to ICIs and TKIs.

Keywords: predictive biomarkers in NSCLC; NTRK/PD-L1 status; whole exome sequencing NGS (WES)

Check for updates

Academic Editors: Bruce Fernando Sabath and Mohd W. Nasser

Received: 17 February 2026
Revised: 23 June 2026
Accepted: 3 July 2026
Published: 15 July 2026

Copyright: © 2026 by the authors. Licensee MDPI, Basel, Switzerland. This article is an open access article distributed under the terms and conditions of the Creative Commons Attribution (CC BY) license.

1. Introduction

Lung cancer remains the leading cause of cancer-related mortality worldwide, accounting for approximately 27% of cancer deaths, with non-small cell lung cancer (NSCLC)

representing 83% of cases. Among its histological subtypes, adenocarcinoma predominates (38.5%) [1]. Despite advancements in early detection, prognosis remains poor, with a life expectancy rarely exceeding 24 months [2,3].

Conventional strategies, including surgery for early and locally advanced stages and platinum-based chemotherapy for advanced disease, have been the mainstay of therapy. However, precision medicine has introduced molecularly targeted therapies, significantly improving survival outcomes [4]. Among these, immune checkpoint inhibitors (ICIs) targeting programmed cell death protein 1 (PD-1) and programmed cell death ligand 1 (PD-L1) have shown substantial benefits, achieving survival rates of approximately 30% in NSCLC. PD-1 is an immune checkpoint receptor found on activated T cells, while PD-L1 is expressed on tumor and immune cells. Their interaction suppresses T cell activity, enabling tumors to evade immune detection. ICIs disrupt this interaction, restoring the immune response against cancer cells [5]. However, their effectiveness is reduced in tumors with *EGFR*, *ALK*, or *ROS1* mutations due to low PD-L1 expression and reduced CD8+ T-cell infiltration, or that harbor dysfunctional CD8+ populations. In contrast, patients with *KRAS*, *BRAF*, or *MET* mutations show a more favorable response because they are typically associated with a high tumor mutational burden (TMB)—except in cases where co-mutations with *STK11* are present [4]. The combined therapeutic potential in *NTRK*-altered NSCLC remains uncertain due to its rarity and limited clinical data.

Several monoclonal antibody-based ICIs, such as pembrolizumab, have demonstrated superior efficacy and lower toxicity compared to chemotherapy, particularly as first-line treatments. Phase III trials such as KEYNOTE-010 and CheckMate-057 have confirmed the benefits of anti-PD-1 and anti-PD-L1 agents (e.g., atezolizumab) over docetaxel in second-line settings [6,7]. However, PD-L1 immunohistochemistry (IHC) remains challenging due to variability among monoclonal antibody clones, resulting in inconsistent staining. Blueprint studies aimed at standardizing pathology reporting introduced the 73-10 clone for avelumab, demonstrating high sensitivity in detecting PD-L1 expression [8,9]. Beyond ICIs, novel molecular targets include tyrosine kinase inhibitors (TKIs), such as larotrectinib and entrectinib, which are approved for tumors harboring *NTRK* gene fusions [10–13].

Pan-TRK overexpression results in the constitutive activation of TRKA, TRKB, or TRKC receptors, which bind neurotrophins including NGF, BDNF, NT-3, and NT-4, and trigger oncogenic signaling pathways (RAS/ERK, AKT/mTOR, PKC/PLCγ) involved in cell growth, metabolism, proliferation, and survival [14–18]. *NTRK* has been involved in the genesis and development of more than 14 groups of tumors, including lung cancer [19], although its rearrangement frequency in NSCLC remains low (<0.5%) [20–22]. Accurate detection requires at least two complementary assays, IHC for protein overexpression and a molecular test, such as next-generation sequencing [23] for molecular confirmation of rearrangements [24–30].

The integration of ICIs and TKIs in NSCLC treatment has revolutionized therapeutic strategies. However, few studies have examined the relationship between PD-L1 expression and pan-TRK-overexpressing tumors. Preclinical studies combining ICIs with novel immunomodulatory agents—including Indoleamine 2,3-dioxygenase (IDO) inhibitors and anti-CTLA-4 blockers—have demonstrated efficacy by enhancing the cytotoxic activity of T lymphocytes against tumor cells [31]. This has also led to considering targeting *MAPK*, *BRAF* mutations, or combining anti-PD1 with other inhibitors to optimize therapeutic outcomes [32]. Given the potential therapeutic implications, the question arises whether each of these mutations should be included in biomarker diagnostic reports, along with information on their functional ramifications. This could be particularly important for identifying potential treatments or clinical trials that may benefit the patient, based on published evidence of therapeutic responses. Providing this information may contribute to

enhancing personalized treatment strategies and patient outcomes, particularly given the resistance observed to both types of drugs [12,31].

Likewise, thanks to high-throughput sequencing technologies, recent research has identified oncogenic and/or druggable gene fusions in approximately 3% to 6% of solid tumor cases [33]. Therefore, research should prioritize a better understanding of driver interactions, their metabolic pathways, and responses to immunotherapy—using in vitro, in vivo, and, increasingly, in silico models, which have recently become more significant. In silico protein expression analyses employ computational tools to predict, quantify, and analyze protein expression under various biological conditions. These analyses utilize databases, simulations, structural modeling, data mining, and artificial intelligence algorithms to study protein interactions, functions, and potential biomarkers [34].

This study aims to conduct an in silico analysis of prior research on NTRK and PD-L1 expression, combined with our NSCLC case cohort, to investigate potential correlations with signaling pathways and optimize treatment strategies. Given that response rates to PD-1/PD-L1 inhibitors range from 20% to 90% across various cancers [35], a deeper understanding of how these immune markers interact with molecular drivers is essential for refining precision oncology strategies.

2. Materials and Methods

2.1. Study Cohort and Controls

A total of 482 patients who underwent curative lung tumor surgery between 1987 and 2005 at Karolinska University Hospital were selected for a clinicopathological analysis. Archival formalin-fixed paraffin-embedded (FFPE) specimens from lobectomies were used and processed according to standard procedures. Clinicopathological data were gathered from medical records and pathology reports. Tumors were restaged based on the 8th edition of the UICC/AJCC staging system. Ethical approval was obtained from Karolinska University Hospital: No. 2005/588-31/4 + Amendment 2008/136-32, ensuring compliance with the Declaration of Helsinki.

2.2. TMA Construction and Immunohistochemistry

Archival formalin-fixed paraffin-embedded (FFPE) surgical tumor specimens were collected and arranged into tissue microarrays (TMAs), each comprising duplicate 1 mm cores from both central and peripheral tumor regions. Immunohistochemical staining was performed using anti-PD-L1 clones, 22C3 (Dako, Carpinteria, CA, USA), 28-8 (Abcam, Cambridge, UK), SP142 (Ventana, Roche Diagnostics, Basel, Switzerland), and SP263 (Ventana) following established protocols, using the Dako Link 48 platform (Dako). For pan-TRK detection, 4 µm tissue sections were stained with clone EPR17341 (Abcam) on the Ventana Benchmark Ultra platform (Ventana Medical Systems, Tucson, AZ, USA). Standard immunostaining protocols were followed, including proteolytic pretreatment and antibody incubation, with optimized staining conditions of 56 min at 36 °C. The OptiView DAB kit (Ventana Medical System, Tucson, AZ, USA) was used for signal amplification following cell conditioning at 100 °C for 72 min (CC1, pH 8) per manufacturer guidelines, with an antibody concentration of 30 µg/mL (1:50 dilution). Positive controls included muscle and nerve tissue, while negative controls consisted of kidney, liver, pancreas, and colon tissue within each block.

2.3. Evaluation of PD-L1 Expression

Tumor proportion score (TPS) was determined by evaluating PD-L1 membrane expression in the tumor cells within FFPE-stained samples containing at least 100 tumor cells in the assessment. TPS was classified into three categories: <1% (score 0), ≥1%–<50%

(score 1), and ≥50% (score 2). A score of 0 was considered negative, while scores of ≥1% were categorized as positive. "High expression" was defined as TPS ≥ 50% (Figure 1).

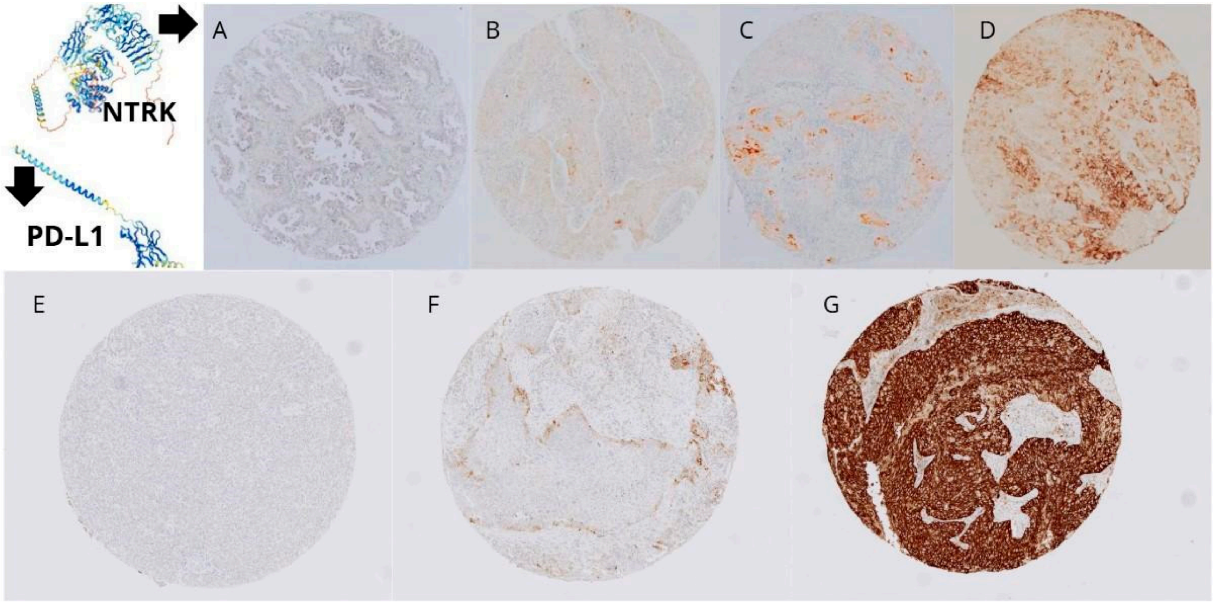


Figure 1. Immunohistochemical detection of Programmed Death-Ligand 1 (PD-L1) expression in NSCLC tissue microarray (TMA) cores using the clone SP263, and NTRK (pan-TRK, EPR17341 clone Abcam). Composition performed with a Hamamatsu scanner. (**A**) corresponds to an AdCa score 0 (7.93×), (**B**) is a SqCC with score +1 (8.12×), (**C**) is a SqCC with score +2 (7.69×) for NTRK, and (**D**) is a SqCC with score +3 (7.91×). (**E**–**G**) correspond to TPS <1%, 1 to <50% and TPS 50% PD-L1 clones, respectively (10×).

PD-L1 expression in tumor cells was analyzed using the viewer PathoZoom® DigitalLab—Core 7.6.4 (Smart in Media AG, Cologne, Germany) software following slide scanning with a Hamamatsu S360 scanner. Pathologists independently assessed the slides without automated assistance. For each case, two TMA cores were examined, and TPS was assigned accordingly. If one core was missing, the remaining core was used for scoring. The final TPS was calculated as the average of the individual scores.

2.4. Evaluation of NTRK Expression by IHC

Two pathologists independently performed blinded assessments of pan-TRK expression in TMA samples, evaluating staining patterns in the membrane, cytoplasm, and nucleus. A minimum of 100 tumor cells was required for analysis, and the proportion of stained tumor cells was quantified using the TPS. Staining intensity was categorized as follows: Score 0 for no staining, score 1 for low-intensity staining in >1–10% of tumor cells, score 2 for moderate staining in 10–50% of tumor cells, and score 3 for high-intensity staining in >50% of tumor cells (Figure 1).

In cases of discordant results, a harmonization score was applied. Digital images of TMAs were analyzed using the viewer PathoZoom® DigitalLab—Core 7.6.4 (Smart in Media AG) software following slide scanning with a Hamamatsu S360 scanner. The core with the highest score was considered the most representative; if one core was missing, the remaining cores were used for scoring. The final score was calculated by averaging the pathologists' evaluations.

2.5. Sample Preparation for Whole Exome Sequencing and Bioinformatics Analysis

High molecular weight DNA was isolated from formalin-fixed, paraffin-embedded (FFPE) tumor tissues obtained from 22 NSCLC patients who were positive in IHC for pan-

TRK using the AllPrep DNA/RNA FFPE kit from Qiagen (Hilden, Germany) following the manufacturer's protocol [36]. The genomic DNA was randomly fragmented into short segments sized between 180–280 bp, then underwent end repair, A-tailing, and ligation with Illumina adapters. The adapter-bound fragments were PCR amplified, size-selected, and purified. Subsequently, the captured libraries underwent PCR enrichment, and the quantified libraries were pooled and sequenced on an Illumina Novaseq 6000 using a PE150 strategy. Throughout the process, Qubit and real-time PCR were utilized for quantity and quality control, while the bioanalyzer was employed for size distribution analysis.

The analysis pipeline adhered to Genome Analysis Toolkit (GATK, Cambridge, MA, USA) best-practice guidelines. Fastq files were assessed using FastQC (v 0.11.9), and adapter removal and quality-based trimming were performed using Trim-galore (v 0.6.6). Clean paired-end reads were aligned to the GRCh38.p13 human genome reference using the Burrows–Wheeler Aligner (BWA) [37]. SAMtools (v. 1.9) was utilized for binary alignment map (BAM) file filtering, and Picard was employed for duplicate read marking [38]. Variant calling was conducted using Deepvariant in whole-exome sequencing mode [39], and Vcftools (v 0.1.16) was used for variant retention, with intersectBed (v 2.30.0) keeping only exon variants. SnpEff (v 4.3) facilitated variant annotation [40]. The maftools R package v 2.22.0 was employed for mutation summary, analysis, and visualization using mutation annotation format (maf) files [41]. Gene fusions were inspected, visualized, and identified using the Integrative Genomics Viewer (IGV) web app (Cambridge, MA, USA) [42].

2.6. In Silico and Literature Analysis for Non-Canonical Variants

Canonical and non-canonical variants of PD-L1, NTRK and other related molecules were analyzed in silico with the following tools, which provide literature and predictions on protein function, protein interactions, pathways, protein structure and protein expression: STRING databases [43], BioGRID database [44], IntAct [45], KEGG Pathway [46], Reactome [47], WikiPathways [48,49], Database Commons [50], InterPro [23,51], PhosphoSitePlus [52], RCSB Protein Data Bank [53], Panther database [54], The Human Protein Atlas [55,56], Drugbank [57], Drug-Gene Interaction Database (DGIdb) v 5.0.8 [58] and Network figures were drawn with Cytoscape program v 3.10.3 [59–61].

2.7. Statistical Analysis

Statistica, TIBCO Software Inc. (2020) (Palo Alto, CA, USA). Data Science Workbench, version 14 (http://tibco.com), and IBM SPSS Statistics 29 software were utilized for statistical analyses. Overall survival (OS) served as the primary outcome measure. Survival analysis included Kaplan–Meier curves (log-rank test), Cox regression, and crosstabulation for subgroups based on antibody positivity. Age and sex were adjusted in multivariate Cox regression. Associations between variables were assessed using the $\chi 2$ statistic. A p-value of <0.05 was considered to be significant. Variables from univariate and multivariate analyses were explored as prognostic factors.

3. Results

3.1. Patient and Tumor Characteristics

In total, 482 patients were studied. The median age was 68 years (39–86), and smoking status was documented for 90% of the patients, with 53.4% identified as current smokers. The sex ratio was male:female of 1.2:1. The histological subtypes included adenocarcinoma (AdCa) (60.6%), squamous-cell carcinoma (SqCC) (33%), and large cell carcinoma (LCC) (6.4%). The pT (extent of the tumor) category was as follows: T1 (36%), T2–T4 (64%). The p-stage was as follows: IA (37.2%), IB (39.6%), IIA (10.2%), IIB (11.4%), IIIA (1.2%), IIIB–IV (0.4%), with Grade 3 being the most predominant (43.2%) [62].

3.2. PD-L1 Immunohistochemical Staining

Previous investigations from our group have established the relevance of PD-L1 in NSCLC [63], with positivity (TPS $\geq$ 1%) observed in 41.5% for clone 28-8, 34.2% for 22C3, 42.7% for SP263, and 10.4% for SP142 ($p < 0.0001$). Similarly, high PD-L1 expression (TPS $\geq$ 50%) was detected at 14.1% for 28-8, 13.1% for 22C3, 16.2% for SP263, and 3.9% for SP142 ($p < 0.0001$). Likewise, the expression was significantly higher at advanced pT stage and histological grade ($p < 0.05$ and $p < 0.012$), being slightly different for the histological type, with SqCC being more frequent when TPS $\geq$ 50% ($p = 0.0001$).

3.3. TRK Immunohistochemical Staining

In previous observations, most tumor samples exhibited negative pan-TRK expression. Positive staining was observed in 22 out of 482 cases (4.56%). The non-tumoral lung tissue did not display TRK expression. There were occasionally some lymphocytes and macrophages with weak staining. TRK expression was more frequently detected in SqCC in 16/22 (72.72%) than in AdCa 3/22 (13.6%). Additionally, we discovered expression in 3/22 LCC (13.6%), corresponding to 3.3%, 0.6%, and 0.6% of all lung cancer cases, respectively. The majority of the staining was cytoplasmic and membrane-based. There was no nuclear or perinuclear staining in any of the instances [62,64].

3.4. Correlation Between TRK and PD-L1 Immunohistochemical Expression in Tumor Cells and Clinicopathological Findings and Patient Prognosis

A statistically significant association was observed between PD-L1 expression using clone SP142 (TPS $\geq$ 50%) and overall survival (OS) in NSCLC and Non-adenocarcinoma (non-AdCa) based on Kaplan–Meier analysis (log-rank $p = 0.045$ and $p = 0.05$, respectively). Additionally, OS was associated with PD-L1 expression in patients with LCC, as assessed by clones 22C3 and SP263. Patients with a TPS < 50% had better OS compared to those with a TPS $\geq$ 50% (log-rank $p = 0.009$ and $p = 0.05$, respectively) in all clones. No significant association between PD-L1 expression and OS was found in NSCLC using clones 28-8, 22C3, and SP263.

Multivariate analysis using Cox regression revealed that in NSCLC and Non-AdCa, PD-L1 tumor positivity (TPS $\geq$ 50%) with clone SP142 could serve as an independent prognostic factor among various variables ($p = 0.043$ and $p = 0.042$, respectively). Furthermore, in Non-AdCa, PD-L1 expression $\geq$ 50% with clone 22C3 also appeared to be an independent prognostic factor ($p = 0.006$). Similarly, in LCC, multivariate analysis indicated that PD-L1 expression $\geq$50% in tumor cells was an independent prognostic factor when assessed with clones 22C3, 28-8, SP263, and SP142 ($p = 0.010$, $p = 0.029$, $p = 0.008$, and $p = 0.017$, respectively). No significant associations were observed in AdCa or SqCC. Additionally, the analysis was applicable to all LCC clones with TPS $\geq$ 50%, age (except the SP263 clone), and TNM stage. TNM stage is directly linked to survival ($p < 0.001$), and not to grade or histological type. Despite this, grade 1 tumors appeared to have better survival rates. In an analogous but disparate way, positive TRK expression in NSCLC correlated significantly with histological subtypes ($p < 0.001$), particularly SqCC ($p = 0.038$), and grade of differentiation ($p = 0.036$). However, staining intensity did not reach significance. No correlations were found with age, tumor size, or overall survival. Additionally, there was no statistically significant association between pan-TRK staining and overall survival (OS) using Kaplan–Meier analysis (log-rank $p = 0.821$) [62,63]. It is worth noting that when TNM stage was incorporated into the multivariable Cox model alongside age and sex, neither PD-L1 clone nor NTRK expression reached independent prognostic significance, reflecting the near-uniform early-stage distribution in this surgical cohort (98.4% Stage I–II). Additionally, findings in the LCC subgroup ($n \approx 31$) should be interpreted with caution

due to limited statistical power. These survival analyses should therefore be interpreted as exploratory, and the previously reported borderline findings require validation in larger, stage-diverse cohorts.

PD-L1 expression showed a statistically significant correlation with pan-TRK, grade and histology for all clones ($p < 0.001$), where all cases co-expressed both biomarkers except case 1 which was negative for SP142, all LCCs expressed both biomarkers and SP263 was the clone with the highest PD-L1 expression with similar behavior and predominant expression in SqCC and high-grade tumors (G3 63.6% and G2 36.4%) (Figure 2). Pan-TRK staining was present, especially in SqCC, in 3.3% of all samples ($p < 0.001$). In addition, there was a strong correlation between TRK expression and PD-L1 positivity; all 22 TRK-positive samples expressed PD-L1 between 95–100% of the PD-L1 when TPS was >1%, and between 54–95% when TPS was >50% ($p < 0.001$) (Figure 3). Complementary analyses—including multivariable logistic regression adjusted for age, sex, histology, grade, and stage (adjusted OR ranging from 28 to 102 across clones), ordinal logistic modeling, and multiple correspondence analysis (MCA)—consistently confirmed that pan-TRK and PD-L1 co-expression constitutes a structurally independent molecular pattern. Dimension 1 of the MCA (explaining 10.1% of the 19.6% total inertia) was primarily defined by TRK-positive/PD-L1-high co-occurrence, with minimal contribution from the other clinical variables.

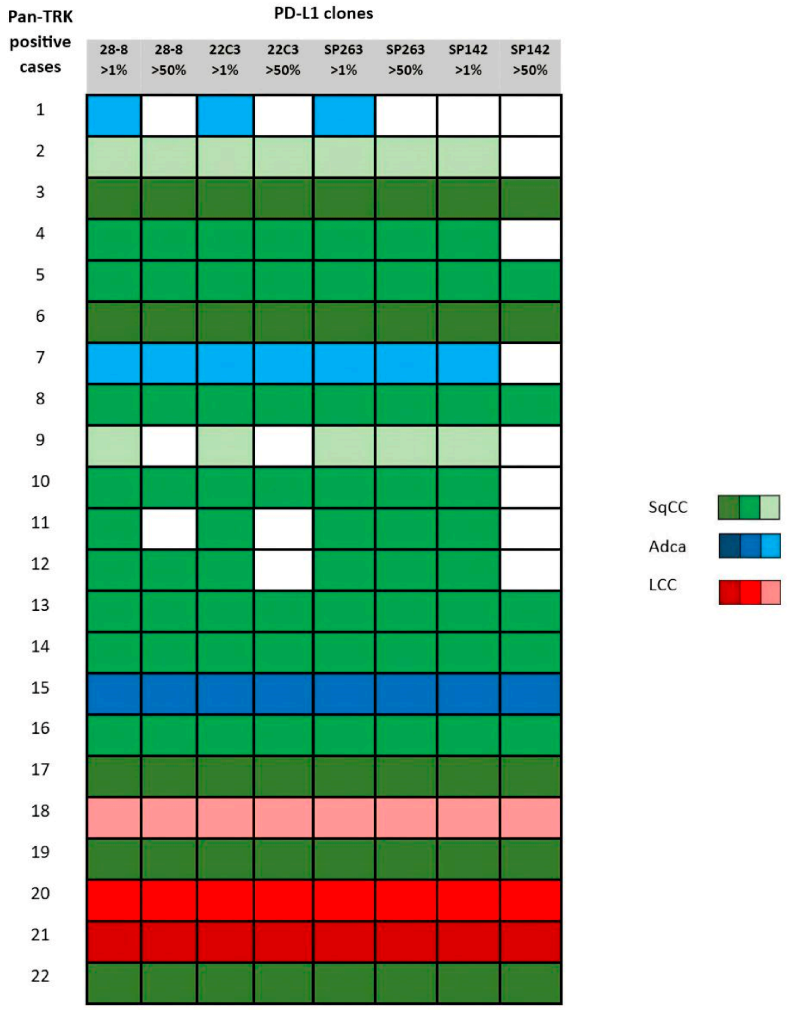


Figure 2. Co-expression heatmap of pan-TRK and PD-L1 in the 22 IHC-positive NSCLC cases. Each row represents an individual case; columns display PD-L1 positivity (TPS > 1% and TPS > 50%) for

four antibody clones (28-8, 22C3, SP263, SP142). Histological subtypes are color-coded: green (SqCC), blue (AdCa), red (LCC). Pan-TRK staining intensity is represented by color shading: dark (+3, strong), medium (+2, moderate), light (+1, weak); white boxes indicate PD-L1 negativity. The predominance of colored cells across all clones and thresholds illustrates the strong and consistent co-expression of pan-TRK and PD-L1, irrespective of histological subtype, with SP263 demonstrating the broadest positivity and SP142 the highest specificity for high-expression cases.

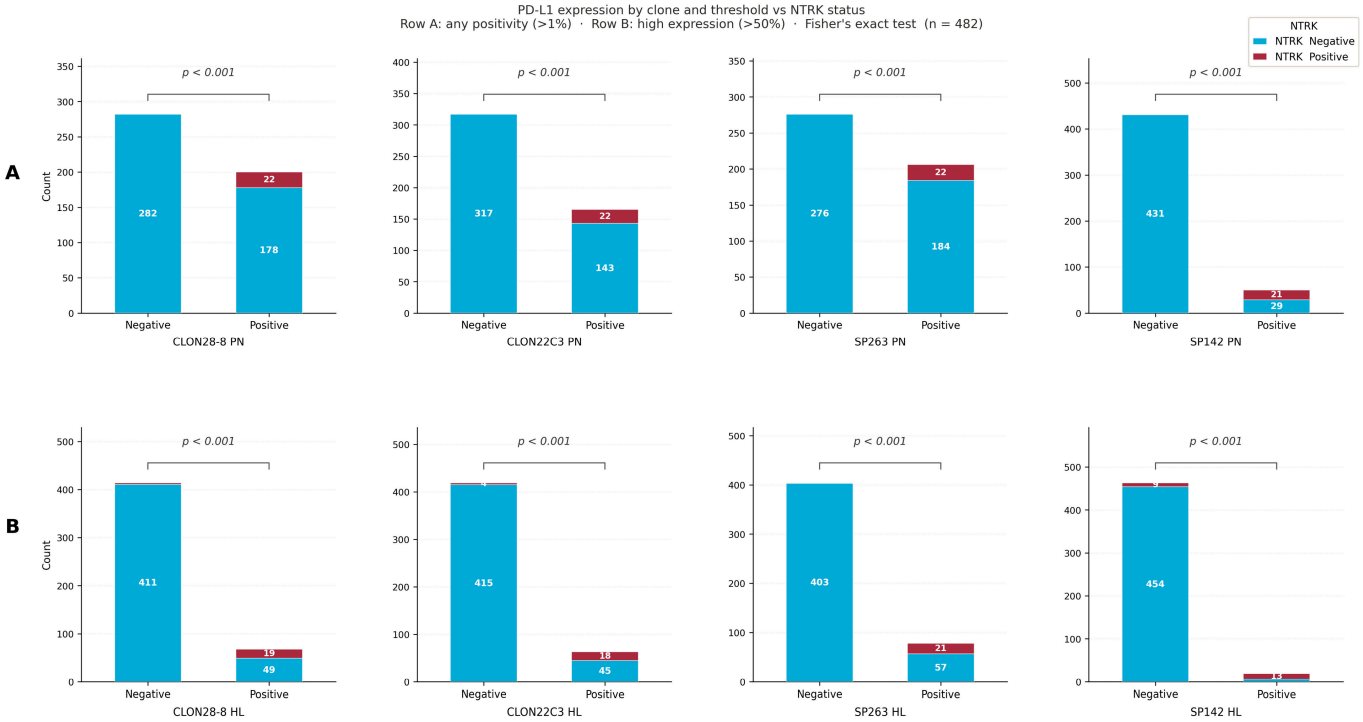


Figure 3. Cross-tabulation between every PD-L1 clone and NTRK. In the figure, there is a statistically significant correlation across all clones, indicating that all positive cases with pan-TRK have PD-L1 expression in most cases. (**A**) PD-L expression > 1%; (**B**) High PD-L1 expression $\geq$ 50%.

3.5. NTRK Somatic Mutations, CNV and Fusions Detected by NGS Analysis

After extracting DNA from FFPE samples, 15 of the 22 pan-TRK positive cases fulfilled quality standards and underwent whole exome sequencing (WES) to identify cancer-related somatic DNA mutations, copy number variations (CNVs), and *NTRK* fusion genes. Seven samples with positive TRK-IHC were excluded from WES due to inadequate DNA extraction and high fragmentation levels, likely due to improper formalin fixation. Somatic variants were identified using strict filters: variant allele frequency (VAF) > 5%, site depth $\geq$ 20, $\geq$5 alternate reads, and exclusion of variants listed in ExAC or gnomAD. Variant call format (VCF) files with annotated somatic mutations were converted to mutation annotation format (MAF) and analyzed with the maftools R package.

Several somatic mutations were identified across 15 pan-TRK–positive samples, most of which correspond to missense mutations, with one stop-gained mutation in *JAK2*, as visualized in the Oncoplot (Figure 4). Notably, *NGFR* deletions and multiple mutations in *MTOR*, *STAT1*, *EGFR*, *SORCS2* (Vps10 receptor linked to Sortilin 1), *NFKBIL1* (NF-κB), and *PDCD1LG2* (PD-L2) were identified in the samples [65–67]. Conversely, *NTRK1* mutations were detected in only one case, along with other somatic mutations in key cancer-associated genes such as *PIK3CA*, *RET*, *KRAS*, *BRAF*, *APC*, and *PTEN* (Table 1). CNV analysis using GISTIC (v 2.0.23) identified amplifications in *NTRK1* and *ERBB2*, with deletions of *TP53* and *NGFR* (Supplementary S1 and S2). Gene rearrangements were detected in 11 samples using the FuSeq WES v 1.0.0 and validated with IGV, with three unique *NTRK* rearrangements detected involving *AFAP1*, *TPM3*, and *RASEF*. *NTRK1* fusions were found in one case,

while *NTRK2* fusions appeared in two cases. No *NTRK3* rearrangements were identified. Additional fusions involving other lung cancer driver genes were detected, including *ALK* (6/15), *ROS1* (2/15), *MET* (2/15), *RET* (1/15), and *NRG1* (1/15). Notably, five cases exhibited dual fusions within the same sample, one of which involved *TPM3—NTRK1* and *ALK—VCL* (Table 1, Supplementary S3). The three *NTRK* rearrangements were identified in two SqCC cases and one AdCa case. All are G2 and G3 and stage I and II, as previously published [64]. In the comparative analysis of PD-L1 expression with the rearrangements, Sample 1 (AdCa) showed an *NTRK2* fusion, *TP53* and *PIK3CA* mutations, +1 pan-TRK staining, and mild PD-L1 expression (10–80% of tumor cells) for all clones except SP142 (negative). Sample 7 (SqCC) presented *NTRK1* and *ALK* fusions, no classic NSCLC driver mutations—but a stop-gained *JAK2* mutation—, +2 pan-TRK staining, and moderate PD-L1 positivity (55–70% of tumor cells) for all clones. Sample 10 (SqCC) had *NTRK2* and *MET* rearrangements, no common NSCLC driver mutations—but multiple somatic mutations in Sortilin 1 and PD-L2—, +3 pan-TRK staining, and strong PD-L1 expression (80–90% of tumor cells) across all clones. Adjusted prevalence with WES NGS was 0.91%.

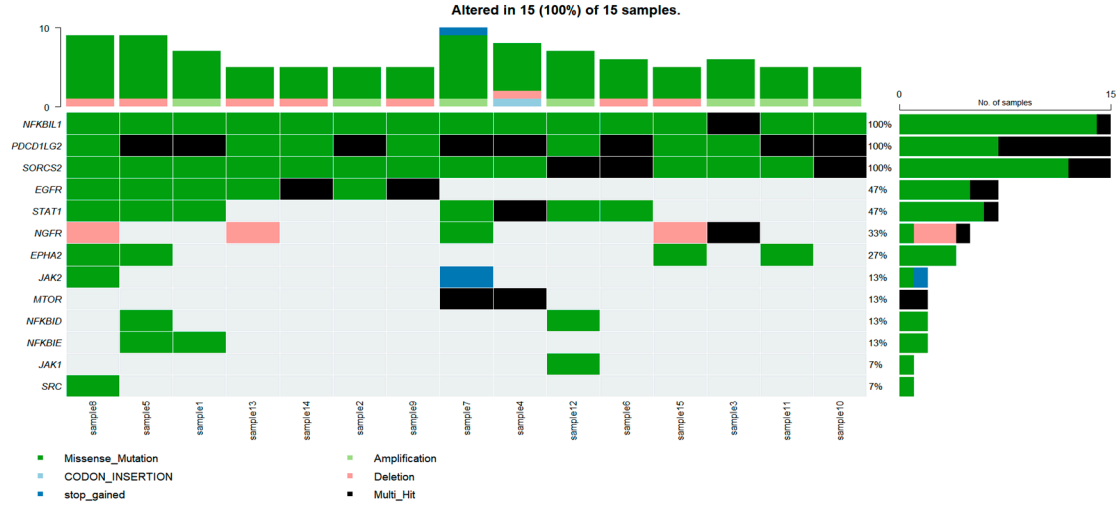


Figure 4. The Oncoplot provides a comprehensive overview of somatic mutations identified across specific genes (rows) in 15 individual patient samples (columns). Mutations are color-coded according to their type. The top bar indicates the total number of mutations detected in each patient, while the side bar denotes the number of patients harboring a given mutation. The bottom panel displays the spectrum of single-nucleotide polymorphism (SNP) transitions and transversions, with bar colors illustrating the distribution of the six possible nucleotide conversions within each sample. Notably, recurrent alterations were observed in *NFKBIL1* (NF-κB), *PDCD1LG2* (PD-L2), *SORCS2* (sortilin 1), *EGFR*, and *MTOR*, accompanied by deletions in *NGFR* (p75NTR) and a stop-gained variant in *JAK2*.

The table summarizes each *NTRK* fusion present in the samples and its grade of immunohistochemical staining, implicated chromosome partners, histological type, and other somatic mutations and PD-L1 staining grade.

Table 1. *NTRK* rearrangements and driver fusion partners, somatic mutations, pan-TRK and PD-L1 expressions. Molecular and immunohistochemical characterization of the 15 pan-TRK-positive NSCLC cases analyzed by whole-exome sequencing (WES). Gene fusions are shown with their respective chromosomal partners, histological subtype, and pan-TRK staining intensity (score 1–3). PD-L1 expression is reported for four antibody clones (28-8, 22C3, SP263, SP142) using a semiquantitative score: 0 (TPS < 1%), 1 (TPS ≥ 1–<50%), 2–3 (TPS ≥ 50%). Additional somatic mutations in cancer-relevant genes are indicated; asterisks (*) denote co-occurring tumor suppressor alterations. Cases with confirmed NTRK1 or NTRK2 fusions consistently demonstrate concurrent PD-L1 positivity across all clones, supporting their biological co-expression.

Cases	Sample 1 Case 1	Sample 2 Case 3	Sample 3 Case 6	Sample 4 Case 7	Sample 5 Case 10	Sample 6 Case 11		Sample 7 Case 12		Sample 8 Case 14		Sample 9 Case 15	Sample 10 Case 17		Sample 11 Case 18	Sample 12 Case 19	Sample 13 Case 20		Sample 14 Case 21	Sample 15 Case 22
Fusion Partner	*AFAP1—*		*ALK—*	*ALK—*	*ALK—*	*ALK—*	*ALK—*	*TPM3—*	*ALK—*	*ALK—*	*ROS1—*	*PCM1—*	*RASEF—*	*MET—*		*RET—*	*ROS1—*	*MET—*		
	NTRK2		*KCNQ5*	*CTLC*	*HIP1*	*HIP1*	*KCNQ5*	*NTRK1*	*VCL*	*HIP1*	*CEP85L*	*NRG1*	*NTRK2*	*KIF5B*		*SPECC1L*	*GOPC*	*CAPZA2*		
Partner 1	Chr4		Chr2	Chr2	Chr2	Chr2	Chr2	Chr1	Chr2	Chr2	Chr6	Chr8	Chr9	Chr7		Chr10	Chr6	Chr7		
Partner 2	Chr9		Chr6	Chr17	Chr7	Chr7	Chr6	Chr1	Chr10	Chr7	Chr6	Chr8	Chr9	Chr10		Chr22	Chr6	Chr7		
Histology	Adca	SqCC	SqCC	Adca	SqCC	SqCC		SqCC		SqCC		Adca	SqCC		LCC	SqCC	LCC		LCC	SqCC
NTRK-IHC	1	3	3	1	2	2		2		2		2	3		1	3	2		3	3
PD-L1 28-8	1	2	2	2	2	1		2		2		2	2		2	2	2		2	2
PD-L1 22C3	1	2	2	2	2	1		1		2		2	2		2	2	2		2	2
PD-L1 SP263	1	2	2	2	2	1		2		2		2	2		2	3	2		2	2
PD-L1 SP142	0	3	3	2	2	2		2		3		3	2		3	3	3		3	3
Other Somatic Mutations	** TP53, PIK3CA*	*APC*			*PTEN*					*APC*					** TP53*	*NTRK1, RET*	*BRAF*			*KRAS*

3.6. In Silico and Literature Analysis for Non-Canonical Variants

Several databases accessed via Database Commons were utilized to explore molecular interactions and signaling pathways involving PD-L1 and TRK receptors in NSCLC. Among these, STRING was instrumental in identifying protein-protein interactions based on experimental data and computational predictions. InterPro and Panther enabled the classification of protein domains, while IntAct and the RCSB Protein Data Bank provided structural and molecular interaction data, including post-translational modifications. Canonical and non-canonical signaling pathways were investigated using KEGG Pathway, Reactome, and WikiPathways, whereas PhosphoSitePlus offered detailed information on phosphorylation events and other post-translational modifications. The Human Protein Atlas was employed to analyze protein expression profiles. DrugBank and DGIdb supplied information on pharmacological agents, including those targeting non-canonical molecules (Supplementary S4). Finally, Cytoscape was used to construct the network. Subsequently, analysis using STRING revealed that the input proteins exhibited significantly more interactions than would be expected by chance for a random set of proteins with similar size and degree distribution in the genome. This enrichment suggests that the proteins are biologically interconnected to some extent. Although minimal enrichment was anticipated due to the small initial input (two or more proteins), STRING, by default, expanded the network to include 30 additional nodes. This inherent extension requires caution when interpreting connectivity, as at least 30 associated interactions are assumed a priori. To improve statistical validity, we reanalyzed the dataset in STRING using the full list of proteins from the beginning and adjusted the network settings by disabling the "first shell" and "second shell" options, producing a preliminary report (Figure 5).

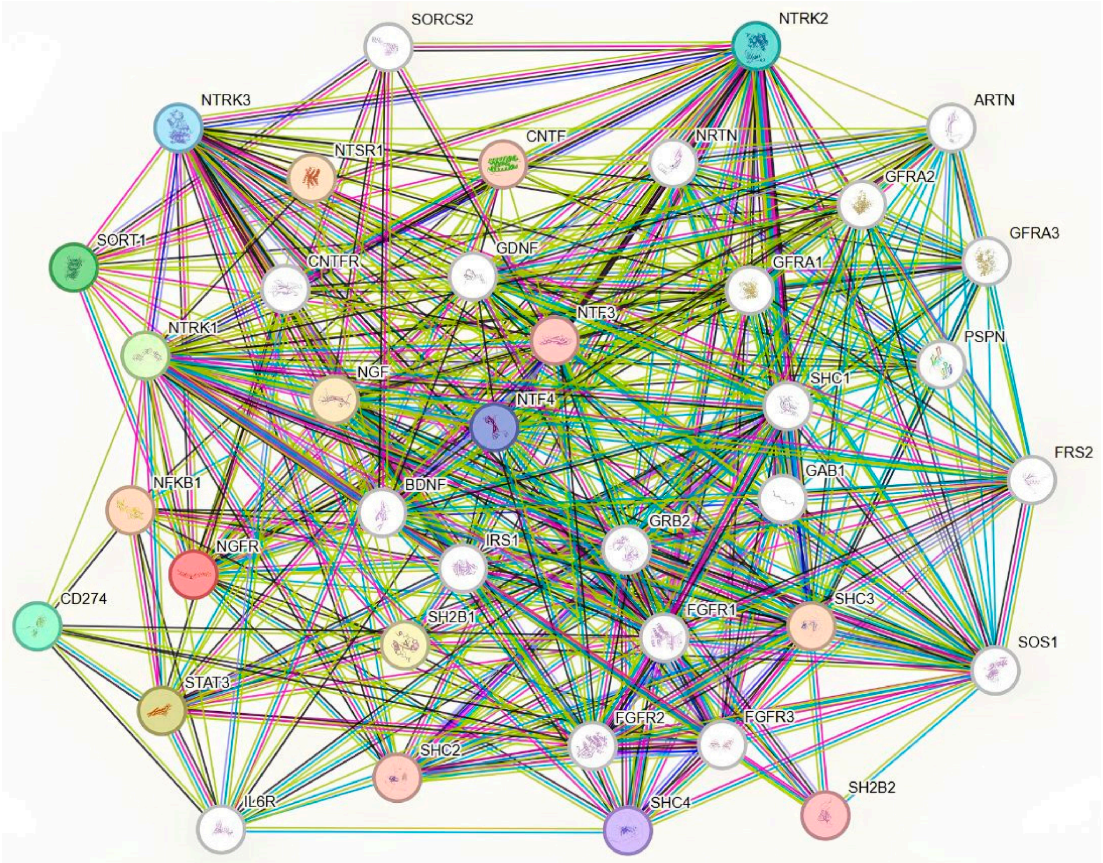


Figure 5. Network created by string-db.org. **ARTN** (Artemin)—Promotes survival and growth of sympathetic neurons. Activates RET pathway; **BDNF** (Brain-Derived Neurotrophic Factor)—Supports neuronal survival and growth. Binds to NTRK2; **CD274** (Programmed Death-Ligand 1, PD-L1)—Inhibits

immune response through T-cell suppression; **CNTF** (Ciliary Neurotrophic Factor)—Promotes neuronal survival; involved in neuroinflammation. Binds CNTFR; **CNTFR** (Ciliary Neurotrophic Factor Receptor)—Receptor for CNTF; mediates neuroprotective effects. Forms a complex with IL-6 and proNGF; **FGFR1** (Fibroblast Growth Factor Receptor 1)—Regulates development, cell growth, and angiogenesis. Activates RAS/MAPK, PI3K/AKT, STAT, and PLCγ pathways; **FGFR2** (Fibroblast Growth Factor Receptor 2)—Involved in cell differentiation and embryogenesis. Activates RAS/MAPK, PI3K/AKT, STAT, and PLCγ pathways; **FGFR3** (Fibroblast Growth Factor Receptor 3)—Regulates bone growth and brain development. Activates RAS/MAPK, PI3K/AKT, STAT, and PLCγ pathways; **FRS2** (Fibroblast Growth Factor Receptor Substrate 2)—Adapter protein in FGFR signaling; **GAB1** (GRB2-Associated Binding Protein 1)—Adapter in growth factor and cytokine signaling. Activates RAS/MAPK, PI3K/AKT, and JNK pathways; **GDNF** (Glial cell line-Derived Neurotrophic Factor)—Supports survival of dopaminergic neurons. Binds GFRA1; **GFRA1** (GDNF Family Receptor Alpha 1)—Co-receptor for GDNF; promotes neuronal development via RET activation; **GFRA2** (GDNF Family Receptor Alpha 2)—Co-receptor for NRTN; supports parasympathetic neurons. Activates RET pathway; **GFRA3** (GDNF Family Receptor Alpha 3)—Co-receptor for ARTN; affects sensory neurons. Activates RET pathway. **IL-6R** (Interleukin-6 Receptor)—Mediates inflammatory and immune responses. STAT3 and SHP2 are associated with AKT pathway activation; **IRS1** (Insulin Receptor Substrate 1)—Transmits insulin and IGF signals. Activates PI3K/AKT and SOS/ERK pathways; **NGF** (Nerve Growth Factor)—Promotes survival of sympathetic and sensory neurons; **NGFR** (Nerve Growth Factor Receptor, p75NTR)—Binds NGF; regulates neuronal survival or apoptosis. Activates Rho/NF-κB and RAS/JNK pathways; **NRTN** (Neurturin)—Supports parasympathetic and enteric neuron survival. Activates RET pathway; **NTRK1** (Neurotrophic Receptor Tyrosine Kinase 1, TRKA)—Receptor for NGF; promotes neuronal survival; **NTRK2** (Neurotrophic Receptor Tyrosine Kinase 2, TRKB)—Receptor for BDNF; promotes neuronal differentiation; **NTRK3** (Neurotrophic Receptor Tyrosine Kinase 3, TRKC)—Receptor for NTF3; supports neuronal survival; **NTSR1** (Neurotensin Receptor 1)—Mediates neurotensin signaling in CNS and periphery. Activates Rho kinases, AKT, and RAS pathways; **NFKB1** (Nuclear Factor kappa-light-chain-enhancer of activated B cells subunit 1)—Regulates immune and inflammatory responses; **NTF3** (Neurotrophin-3, NT3)—Supports neuronal differentiation and survival; **NTF4** (Neurotrophin-4, NT4)—Promotes survival of peripheral sensory neurons; **PSPN** (Persephin)—Supports development of midbrain dopaminergic neurons. Binds GFRA4 and activates RET pathway. **SH2B1** (SH2B Adaptor Protein 1)—Modulates insulin and leptin receptor signaling. Activates RAS, PI3K, and JAK pathways; **SH2B2** (SH2B Adaptor Protein 2)—Enhances receptor tyrosine kinase signaling. Activates RAS pathway; **SHC1** (SHC Adaptor Protein 1)—Couples activated receptors to the RAS signaling pathway; **SHC3** (SHC Adaptor Protein 3)—Involved in neuronal signaling and differentiation. Activates RAS/ERK and PI3K/AKT pathways; **SHC4** (SHC Adaptor Protein 4)—Participates in MAPK signaling in neurons. Activates RAS pathway; **SORCS2** (Sortilin-Related VPS10 Domain Containing Receptor 2)—Modulates neurotrophin signaling and plasticity. Binds p75NTR and BDNF; **SORT1** (Sortilin 1)—Regulates neurotrophin trafficking and receptor internalization. Binds p75NTR; activates JNK pathway; **SOS1** (Son of Sevenless Homolog 1)—Activates RAS; transduces growth factor signals; **STAT3** (Signal Transducer and Activator of Transcription 3)—Mediates responses to cytokines and growth factors.

The refined interaction network was subsequently visualized in Cytoscape using the STRING v 2.2.0 and CytoHubba v 0.1 app plugins. This analysis focused on PD-L1 (CD274) and NTRK1/2/3 and highlighted their connections to canonical signaling pathways, including RAS, MAPK, PLCγ, and PI3K/AKT/mTOR cascades (Figure 6). The research underscores the molecular interactions centered around NTRK1/TRKA, revealing a strong functional association with other TRK family members, neurotrophins, and several co-receptors, particularly those linked to the GDNF signaling axis. Additionally, weaker yet significant connections were observed between NTRK1 and various secondary nodes in the network, notably with intracellular signaling mediators and second messengers. The connection between NTRK1 and PD-L1 appears limited; nonetheless, indirect crosstalk is evident through the NGFR (p75NTR) and STAT3 pathways—activated via interleukin

receptors, especially IL-6. These physical and non-canonical interactions were identified from BioGRID-referenced and curated datasets.

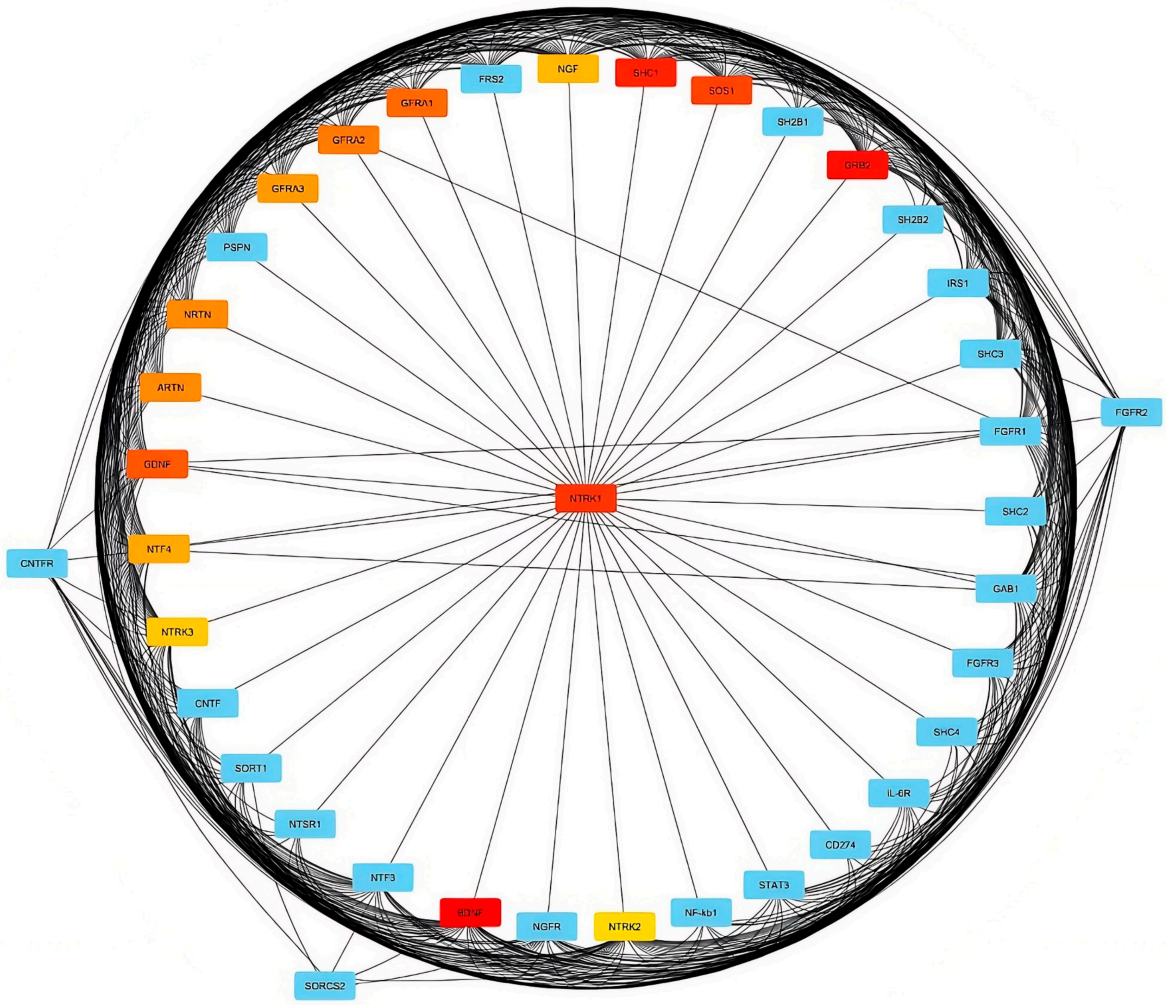


Figure 6. Network created by the Cytoscape program. Using Cytoscape in conjunction with the STRING database enables the identification of key protein nodes within biological interaction networks. In this analysis, the CytoHubba plugin was used with predefined parameters to generate a heatmap highlighting proteins with the strongest predicted associations with NTRK1 (TRKA). The resulting image displays an intensity gradient from red to yellow, indicating decreasing interaction strength. Proteins shown in light blue represent those with weaker or indirect associations—potentially mediated by non-canonical pathways—such as PD-L1.

4. Discussion

Over the past 50 years, the five-year survival rate of NSCLC patients has significantly improved, rising from approximately 10% to 23% [68,69]. First- and second-line treatments, such as TKIs, have been shown to extend survival by approximately one year, a benefit comparable to that of immunotherapy. However, therapies targeting ALK and EGFR offer survival extensions of up to 4 years, while ROS1-targeted therapies can extend survival by more than 6 years [68]. These advancements underscore the importance of personalized therapies based on specific genomic alterations.

With the advent of ICIs and TKIs in the last decade, a new era of therapeutic optimism has emerged for patients with lung cancer [70,71]. Higher PD-L1 expression has been associated with increased survival in patients treated with ICIs. When PD-L1 expression is below 50%, median survival is approximately 9 months, whereas patients with expression levels above 50% have a survival exceeding 26 months [8]. However, the appearance

of resistance in such a short period of time raises many questions about how these new molecules work and, in particular, how they can interact with each other and, even more importantly, the feasibility of combining them in individualized treatment strategies.

An alternative approach to investigating these resistance mechanisms has been proposed in this study, where we observed a significant correlation between NTRK and PD-L1 expression by both immunohistochemistry and molecular analyses, particularly in SqCC and high-grade tumors. All 22 TRK-positive cases co-expressed PD-L1, with positivity rates of 95–100% when TPS > 1% and 54–95% when TPS > 50% ($p < 0.001$). While TRK expression alone was not prognostic for OS, PD-L1 positivity (TPS $\geq$ 50%)—particularly when assessed using the SP142 clone—emerged as an independent prognostic factor in NSCLC and non-AdCa subtypes and showed additional predictive value in LCC when multiple clones were evaluated. These findings suggest that PD-L1 and TRK should be evaluated jointly rather than independently, as their co-expression may offer enhanced prognostic precision.

In the genomic analyses, whole-exome sequencing of TRK-positive tumors revealed several interesting alterations. Alongside amplifications in *NTRK1* and *ERBB2*, and deletions in *TP53* and *NGFR* (p75NTR), we identified multiple mutations in *MTOR*, *STAT1*, *EGFR*, *SORCS2*, *NFKBIL1* (NF-κB), and *PDCD1LG2* (PD-L2), as well as a stop-gained mutation in *JAK2*. *NTRK* rearrangements were detected in 3/15 sequenced cases (*NTRK1* and *NTRK2*), while *ALK*, *ROS1*, *MET*, *RET*, and *NRG1* fusions were also present, with several dual rearrangements observed in single samples. Importantly, three illustrative cases demonstrated how *NTRK* fusions co-occurred with additional alterations (e.g., *TP53*, *PIK3CA*, *JAK2* stop-gain, *PD-L2* mutations) and PD-L1 positivity ranging from mild to strong. This strengthens the notion that TRK/PD-L1 interactions are biologically relevant in NSCLC and may reciprocally influence immunotherapy responses.

Mechanistically, these results align with in silico predictions and literature, suggesting that TRK-mediated signaling may upregulate PD-L1 expression through non-canonical pathways involving p75NTR, STAT3, and NF-κB. STAT3, acting as a transcription factor, in particular, binds the PD-L1 promoter, and its activation via ephrin (EPHA and B) signaling—whose pathways are still poorly categorized—may contribute to PD-L1 overexpression [72]. In parallel, NF-κB activation—potentially triggered via TRKA/p75NTR signaling, either by mutation or dimerization—further enhances PD-L1 expression [66,73–76]. Moreover, STAT3 directly binds to NF-κB, retaining it within the nucleus and promoting sustained NF-κB activation in cancer [75,76] (Figure 7). This creates an immunosuppressive tumor microenvironment (TME) that favors CD8+ T cell exhaustion and therapeutic resistance. Interestingly, our data also support previous findings that NTRK1 activation in TILs may contribute to immune dysfunction through the JAK/STAT pathway, a process that can be partially reversed after TKI treatment [31,77]. Similar findings can be observed in *NTRK1* mutations/rearrangements in tumor cells, where TRKA signaling leads to sustained STAT3 activation, promoting tumor progression and treatment resistance. In contrast, although NTRK2 and NTRK3 can also activate STAT3, a definitive association with NSCLC remains controversial [64,77–79].

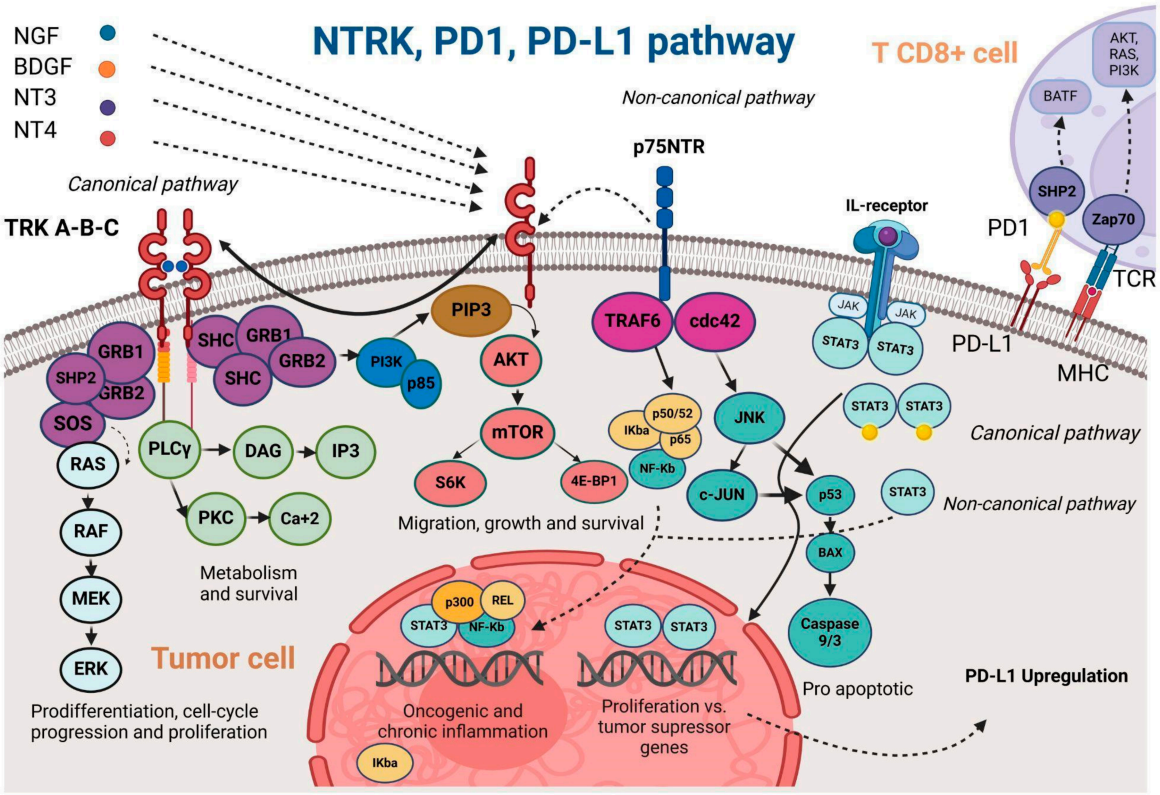


Figure 7. The image provides an overview of the cellular signaling pathways involving NTRK, PD-1, and PD-L1 in lung cancer. Solid arrows represent canonical pathways, while dashed arrows indicate non-canonical routes. Notably, NTRK dimerization with p75NTR predominantly activates canonical second messengers such as RAS and AKT; however, under certain conditions, it can also engage non-canonical pathways, influencing NF-κB activity. STAT3 can be activated by IL-6, PD-L1, and NTRK (particularly TRKA), all of which contribute to the upregulation of PD-L1 expression. The image was created in BioRender.com.

Notably, *PDCD1LG2* mutations detected in our cohort deserve further attention. Given that PD-L2 binds PD-1 with 2–6-fold higher affinity than PD-L1, differential blockade by anti-PD-1 versus anti-PD-L1 therapies could yield distinct outcomes [80]. This could reflect greater PD-L1 activity in those samples in which PD-L2 is mutated. Furthermore, the TMB was relatively high across samples, a feature that typically correlates with increased neoantigen formation and, consequently, enhanced responsiveness to ICIs [78,81]. Nonetheless, clinical responses have also been observed in tumors with low PD-L1 expression, raising concerns about the reliability of PD-L1 as a predictive biomarker [35,63]. Similarly, alterations in NGFR and Sortilin-1, both involved in TRK signaling, highlight the need to broaden the scope of immune checkpoint research beyond PD-L1.

Finally, PD-L1 expression in tumors with *ALK*, *ROS1*, and *NTRK* rearrangements may vary in its predictive value for response to ICIs in solid tumors. Although overexpression is uncommon in *ROS1*- and *NTRK*-rearranged cases, some cohorts with *ALK* fusions have shown PD-L1 upregulation in fewer than 20% of cases [82]. Other studies, however, have indicated that immune escape mechanisms for these rearrangements may lead to increased PD-L1 expression in NSCLC patients with aggressive tumor phenotypes, leading to poor prognosis despite TKI therapy [83].

Despite meeting several Bradford Hill criteria for causality [84,85], our study presents certain limitations. These include its retrospective design, the lack of treatment response evaluation, limited sample size, incomplete WES coverage—chosen over RNA-based NGS for its broader yield from limited archival material, despite RNA-seq remaining the

conventional standard for fusion detection—and use of TMAs, which may underestimate intratumoral heterogeneity. Technical issues such as paraffin block age and environmental factors can also affect PD-L1 staining reliability [80]. Additionally, the study design did not allow for extensive experimental validation, and separate analyses of TRKA, TRKB, and TRKC were not performed—a step that could have improved molecular categorization and strengthened causal inference. While our in silico interactome analyses generated valuable hypotheses, experimental validation of the proposed non-canonical pathways (e.g., TRKA–p75NTR–STAT3/NF-κB) remains necessary. WES-confirmed NTRK rearrangements are low. However, this pattern is consistent with what is expected for low-prevalence, screening-based biomarkers: pan-TRK IHC has high sensitivity but imperfect specificity, and a substantial drop-off between IHC positivity and molecular confirmation is well documented in the literature [24–30]. IHC could be regarded as a screening tool, and molecular confirmation must be mandatory before any targeted therapeutic decision.

Nevertheless, our findings reinforce a biological connection between TRK signaling and PD-L1 expression. The consistent co-expression of TRK and PD-L1, the detection of novel mutations in *JAK2*, *PD-L2*, *NGFR*, *NFKBIL1*, and *SORCS2*, and the identification of *NTRK* fusions alongside *ALK* and *MET* rearrangements point to a complex network of immune evasion mechanisms. Joint evaluation of NTRK and PD-L1 expression may yield more accurate prognostic information and help identify patients likely to develop resistance to immunotherapy or to benefit from combined targeted approaches.

Further studies should explore cytolytic activity, immune checkpoint dynamics and the role of the inflammatory component within the TME, integrating both in vivo and in vitro approaches. However, in silico studies should remain a priority, as they provide a cost-effective strategy to elucidate the molecular mechanisms underlying NTRK overexpression, PD-L1 upregulation, and resistance to immunotherapy. Moreover, computational interactome analyses can substantially reduce research costs by enabling better experimental design and hypothesis refinement.

5. Conclusions

Systematic mapping of TRK interactions is fundamental and opens up new possibilities for research in cell biology and personalized medicine. By integrating this data with additional information on cancer types and therapeutic applications, testable hypotheses about the molecular regulation of TRK can be generated [86]. Interactome analysis is a necessary and integral resource for future research into TRK signaling and opens the door to exploring new insights into TRK function and less-explored functional interactions in the context of cancer and other diseases.

Our findings contribute preliminary, hypothesis-generating evidence suggesting that the co-expression of PD-L1 and TRK in NSCLC may be biologically relevant in the context of ICI therapy. Based on the observed expression patterns, it is plausible that patients with concurrent TRK and PD-L1 overexpression could represent a subgroup warranting further investigation regarding ICI response, particularly when high TMB is present. Conversely, secondary PD-L1 upregulation through NTRK1 signaling remains a potential mechanism of pharmacological resistance that deserves experimental exploration.

Finally, these findings underscore the complex interplay between NTRK1 signaling, STAT3 activation, and immune evasion, highlighting the therapeutic potential of targeting these pathways in NSCLC. These hypotheses require prospective clinical and mechanistic validation before any therapeutic inference can be drawn.

Supplementary Materials: The following supporting information can be downloaded at: https://www.mdpi.com/article/10.3390/jor6030015/s1, Supplementary S1: CNVs GISTIC; Supplementary S2:

CNV alterations G-Score plot; Supplementary S3: Gene rearrangement; Supplementary S4: KEGG and Wiki-pathway.

Author Contributions: R.G., C.O.-V. and S.E., conceptualization and methodology; L.D.P., collection of samples and clinical data; J.G.-H., investigation, writing—original draft preparation, software, visualization, and formal analysis; G.K. and R.M.F., visualization, validation, software, and data curation; C.O.-V., J.G.-H., G.K., R.G., M.A.M.-F., S.E. and L.D.P., supervision, software, and writing—reviewing and editing. All authors have read and agreed to the published version of the manuscript.

Funding: This research received no external funding.

Institutional Review Board Statement: Karolinska University Hospital granted ethical approval in accordance with the Declaration of Helsinki (No. 2005/588-31/4 + Amendment 2008/136-32, approval date: 27 March 2008).

Informed Consent Statement: Since this was a retrospective study, the ethics committee waived the requirement for informed consent.

Data Availability Statement: The original contributions presented in the study are included in the article/Supplementary Materials. Further inquiries can be directed to the corresponding author.

Acknowledgments: We acknowledge Smart in Media AG (viewer PathoZoom® DigitalLab—Core 7.6.4) for providing the image viewer platform.

Conflicts of Interest: The authors declare no conflicts of interest.

References

1. Reckamp, K.L. *Lung Cancer: Treatment and Research*; Springer International Publishing: Cham, Switzerland, 2018.
2. Morgensztern, D.; Campo, M.J.; Dahlberg, S.E.; Doebele, R.C.; Garon, E.; Gerber, D.E.; Goldberg, S.B.; Hammerman, P.S.; Heist, R.S.; Hensing, T.; et al. Molecularly targeted therapies in non-small-cell lung cancer annual update 2014. *J. Thorac. Oncol.* **2015**, *10*, S1–S63. [CrossRef] [PubMed]
3. Volckmar, A.L.; Christopoulos, P.; Kirchner, M.; Allgäuer, M.; Neumann, O.; Budczies, J.; Rempel, E.; Horak, P.; Glade, J.; Goldschmid, H.; et al. Targeting rare and non-canonical driver variants in NSCLC—An uncharted clinical field. *Lung Cancer* **2021**, *154*, 131–141. [CrossRef] [PubMed]
4. Shang, X.; Zhang, W.; Han, W.; Xia, H.; Liu, N.; Wang, X.; Liu, Y. Efficacy of immune checkpoint inhibitors in non-small cell lung cancer with NTRK family mutations. *BMC Pulm. Med.* **2023**, *23*, 482. [CrossRef] [PubMed]
5. Lin, X.; Kang, K.; Chen, P.; Zeng, Z.; Li, G.; Xiong, W.; Yi, M.; Xiang, B. Regulatory mechanisms of PD-1/PD-L1 in cancers. *Mol. Cancer* **2024**, *23*, 108. [CrossRef] [PubMed]
6. Herbst, R.S.; Baas, P.; Kim, D.-W.; Felip, E.; Pérez-Gracia, J.L.; Han, J.-Y.; Molina, J.; Kim, J.-H.; Arvis, C.D.; Ahn, M.-J.; et al. Pembrolizumab versus docetaxel for previously treated, PD-L1-positive, advanced non-small-cell lung cancer (KEYNOTE-010): A randomised controlled trial. *Lancet* **2016**, *387*, 1540–1550. [CrossRef] [PubMed]
7. Borghaei, H.; Paz-Ares, L.; Horn, L.; Spigel, D.R.; Steins, M.; Ready, N.E.; Chow, L.Q.; Vokes, E.E.; Felip, E.; Holgado, E.; et al. Nivolumab versus Docetaxel in Advanced Nonsquamous Non-Small-Cell Lung Cancer. *N. Engl. J. Med.* **2015**, *373*, 1627–1639. [CrossRef] [PubMed]
8. Kerr, K.M.; Nicolson, M.C. Non-Small Cell Lung Cancer, PD-L1, and the Pathologist. *Arch. Pathol. Lab. Med.* **2016**, *140*, 249–254. [CrossRef] [PubMed]
9. Grote, H.J.; Feng, Z.; Schlichting, M.; Helwig, C.; Ruisi, M.; Jin, H.; Scheuenpflug, J.; Gann, C.-N.; Su, Z.; Reck, M.; et al. Programmed Death-Ligand 1 Immunohistochemistry Assay Comparison Studies in NSCLC: Characterization of the 73-10 Assay. *J. Thorac. Oncol.* **2020**, *15*, 1306–1316. [CrossRef] [PubMed]
10. Drilon, A.; Laetsch, T.W.; Kummar, S.; Dubois, S.G.; Lassen, U.N.; Demetri, G.D.; Nathenson, M.; Doebele, R.C.; Farago, A.F.; Pappo, A.S.; et al. Efficacy of Larotrectinib in TRK Fusion-Positive Cancers in Adults and Children. *N. Engl. J. Med.* **2018**, *378*, 731–739. [CrossRef] [PubMed]
11. Ardini, E.; Menichincheri, M.; Banfi, P.; Bosotti, R.; De Ponti, C.; Pulci, R.; Ballinari, D.; Ciomei, M.; Texido, G.; Degrassi, A.; et al. Entrectinib, a Pan-TRK, ROS1, and ALK Inhibitor with Activity in Multiple Molecularly Defined Cancer Indications. *Mol. Cancer Ther.* **2016**, *15*, 628–639. [CrossRef] [PubMed]
12. Qin, H.; Patel, M.R. The Challenge and Opportunity of NTRK Inhibitors in Non-Small Cell Lung Cancer. *Int. J. Mol. Sci.* **2022**, *23*, 2916. [CrossRef] [PubMed]

13. Cocco, E.; Scaltriti, M.; Drilon, A. NTRK fusion-positive cancers and TRK inhibitor therapy. *Nat. Rev. Clin. Oncol.* **2018**, *15*, 731–747. [CrossRef] [PubMed]
14. Ekman, S. How selecting best therapy for metastatic NTRK fusion-positive non-small cell lung cancer? *Transl. Lung Cancer Res.* **2020**, *9*, 2535–2544. [CrossRef]
15. Reichardt, L.F. Neurotrophin-regulated signalling pathways. *Philos. Trans. R. Soc. Lond B Biol. Sci.* **2006**, *361*, 1545–1564. [CrossRef] [PubMed]
16. Gatalica, Z.; Xiu, J.; Swensen, J.; Vranic, S. Molecular characterization of cancers with NTRK gene fusions. *Mod. Pathol.* **2019**, *32*, 147–153. [CrossRef] [PubMed]
17. Solomon, J.P.; Linkov, I.; Rosado, A.; Mullaney, K.; Rosen, E.Y.; Frosina, D.; Jungbluth, A.A.; Zehir, A.; Benayed, R.; Drilon, A.; et al. NTRK fusion detection across multiple assays and 33,997 cases: Diagnostic implications and pitfalls. *Mod. Pathol.* **2020**, *33*, 38–46. [CrossRef] [PubMed]
18. Amatu, A.; Sartore-Bianchi, A.; Bencardino, K.; Pizzutilo, E.; Tosi, F.; Siena, S. Tropomyosin receptor kinase (TRK) biology and the role of NTRK gene fusions in cancer. *Ann. Oncol.* **2019**, *30*, viii5–viii15. [CrossRef] [PubMed]
19. O'Haire, S.; Franchini, F.; Kang, Y.-J.; Steinberg, J.; Canfell, K.; Desai, J.; Fox, S.; Ijzerman, M. Systematic review of NTRK 1/2/3 fusion prevalence pan-cancer and across solid tumours. *Sci. Rep.* **2023**, *13*, 4116. [CrossRef] [PubMed]
20. Forsythe, A.; Zhang, W.; Strauss, U.P.; Fellous, M.; Korei, M.; Keating, K. A systematic review and meta-analysis of neurotrophic tyrosine receptor kinase gene fusion frequencies in solid tumors. *Ther. Adv. Med. Oncol.* **2020**, *12*, 1758835920975613. [CrossRef] [PubMed]
21. Raman, R.; Ramamohan, V.; Rathore, A.; Jain, D.; Mohan, A.; Vashistha, V. Prevalence of highly actionable mutations among Indian patients with advanced non-small cell lung cancer: A systematic review and meta-analysis. *Asia Pac. J. Clin. Oncol.* **2023**, *19*, 158–171. [PubMed]
22. Parra-Medina, R.; Castañeda-González, J.P.; Montoya, L.; Gómez-Gómez, M.P.; Cabezas, D.C.; Vargas, M.P. Prevalence of oncogenic driver mutations in Hispanics/Latin patients with lung cancer. A systematic review and meta-analysis. *Lung Cancer* **2023**, *185*, 107378. [CrossRef] [PubMed]
23. Mitchell, A.L.; Attwood, T.K.; Babbitt, P.C.; Blum, M.; Bork, P.; Bridge, A.; Brown, S.D.; Chang, H.-Y.; El-Gebali, S.; Fraser, M.I.; et al. InterPro in 2019: Improving coverage, classification and access to protein sequence annotations. *Nucleic Acids Res.* **2019**, *47*, D351–D360. [PubMed]
24. Elfving, H.; Broström, E.; Moens, L.N.; Almlöf, J.; Cerjan, D.; Lauter, G.; Nord, H.; Mattsson, J.S.; Ullenhag, G.J.; Strell, C.; et al. Evaluation of NTRK immunohistochemistry as a screening method for NTRK gene fusion detection in non-small cell lung cancer. *Lung Cancer* **2021**, *151*, 53–59. [CrossRef] [PubMed]
25. Solomon, J.P.; Benayed, R.; Hechtman, J.F.; Ladanyi, M. Identifying patients with NTRK fusion cancer. *Ann. Oncol.* **2019**, *30*, viii16–viii22. [CrossRef] [PubMed]
26. Penault-Llorca, F.; Rudzinski, E.R.; Sepulveda, A.R. Sepulveda, Testing algorithm for identification of patients with TRK fusion cancer. *J. Clin. Pathol.* **2019**, *72*, 460–467. [CrossRef] [PubMed]
27. Wong, D.; Yip, S.; Sorensen, P.H. Methods for Identifying Patients with Tropomyosin Receptor Kinase (TRK) Fusion Cancer. *Pathol. Oncol. Res.* **2020**, *26*, 1385–1399. [PubMed]
28. Zito Marino, F.; Pagliuca, F.; Ronchi, A.; Cozzolino, I.; Montella, M.; Berretta, M.; Errico, M.E.; Donofrio, V.; Bianco, R.; Franco, R. NTRK Fusions, from the Diagnostic Algorithm to Innovative Treatment in the Era of Precision Medicine. *Int. J. Mol. Sci.* **2020**, *21*, 3718. [CrossRef] [PubMed]
29. Solomon, J.P.; Hechtman, J.F. Detection of NTRK Fusions: Merits and Limitations of Current Diagnostic Platforms. *Cancer Res.* **2019**, *79*, 3163–3168. [CrossRef] [PubMed]
30. Marchio, C.; Scaltriti, M.; Ladanyi, M.; Iafrate, A.; Bibeau, F.; Dietel, M.; Hechtman, J.; Troiani, T.; López-Rios, F.; Douillard, J.-Y.; et al. ESMO recommendations on the standard methods to detect NTRK fusions in daily practice and clinical research. *Ann. Oncol.* **2019**, *30*, 1417–1427. [CrossRef] [PubMed]
31. Lei, Q.; Wang, D.; Sun, K.; Wang, L.; Zhang, Y. Resistance Mechanisms of Anti-PD1/PDL1 Therapy in Solid Tumors. *Front. Cell Dev. Biol.* **2020**, *8*, 672. [CrossRef] [PubMed]
32. Overbeck, T.R.; Reiffert, A.; Schmitz, K.; Rittmeyer, A.; Körber, W.; Hugo, S.; Schnalke, J.; Lukat, L.; Hugo, T.; Hinterthaner, M.; et al. NTRK Gene Fusions in Non-Small-Cell Lung Cancer: Real-World Screening Data of 1068 Unselected Patients. *Cancers* **2023**, *15*, 2966. [CrossRef] [PubMed]
33. Berrino, E.; Bragoni, A.; Annaratone, L.; Fenocchio, E.; Carnevale-Schianca, F.; Garetto, L.; Aglietta, M.; Sarotto, I.; Casorzo, L.; Venesio, T.; et al. Pursuit of Gene Fusions in Daily Practice: Evidence from Real-World Data in Wild-Type and Microsatellite Instable Patients. *Cancers* **2021**, *13*, 3376. [CrossRef] [PubMed]

34. Sood, N.; Chaudhary, S.; Pardeshi, T.; Mujawar, S.; Deshmukh, K.B.; Sheikh, S.A.; Sharma, P. In-silico study of small cell lung cancer based on protein structure and function: A new approach to mimic biological system. *J. Adv. Pharm. Technol. Res.* **2015**, *6*, 125–129. [CrossRef] [PubMed]
35. Bardhan, K.; Anagnostou, T.; Boussiotis, V.A. The PD1:PD-L1/2 Pathway from Discovery to Clinical Implementation. *Front. Immunol.* **2016**, *7*, 550. [CrossRef] [PubMed]
36. Patel, P.G.; Selvarajah, S.; Guérard, K.-P.; Bartlett, J.M.S.; Lapointe, J.; Berman, D.M.; Okello, J.B.A.; Park, P.C. Reliability and performance of commercial RNA and DNA extraction kits for FFPE tissue cores. *PLoS ONE* **2017**, *12*, e0179732. [CrossRef] [PubMed]
37. McKenna, A.; Hanna, M.; Banks, E.; Sivachenko, A.; Cibulskis, K.; Kernytsky, A.; Garimella, K.; Altshuler, D.; Gabriel, S.; Daly, M.; et al. The Genome Analysis Toolkit: A MapReduce framework for analyzing next-generation DNA sequencing data. *Genome Res.* **2010**, *20*, 1297–1303. [CrossRef] [PubMed]
38. Li, H.; Durbin, R. Fast and accurate short read alignment with Burrows-Wheeler transform. *Bioinformatics* **2009**, *25*, 1754–1760. [CrossRef] [PubMed]
39. Poplin, R.; Chang, P.-C.; Alexander, D.; Schwartz, S.; Colthurst, T.; Ku, A.; Newburger, D.; Dijamco, J.; Nguyen, N.; Afshar, P.T.; et al. A universal SNP and small-indel variant caller using deep neural networks. *Nat. Biotechnol.* **2018**, *36*, 983–987. [CrossRef] [PubMed]
40. Cingolani, P.; Platts, A.; Wang, L.L.; Coon, M.; Nguyen, T.; Wang, L.; Land, S.J.; Lu, X.; Ruden, D.M. A program for annotating and predicting the effects of single nucleotide polymorphisms, SnpEff: SNPs in the genome of Drosophila melanogaster strain w1118; iso-2; iso-3. *Fly* **2012**, *6*, 80–92. [CrossRef] [PubMed]
41. Mayakonda, A.; Lin, D.-C.; Assenov, Y.; Plass, C.; Koeffler, H.P. Maftools: Efficient and comprehensive analysis of somatic variants in cancer. *Genome Res.* **2018**, *28*, 1747–1756. [CrossRef] [PubMed]
42. Chen, S.; Liu, M.; Huang, T.; Liao, W.; Xu, M.; Gu, J. GeneFuse: Detection and visualization of target gene fusions from DNA sequencing data. *Int. J. Biol. Sci.* **2018**, *14*, 843–848. [CrossRef] [PubMed]
43. Szklarczyk, D.; Gable, A.L.; Lyon, D.; Junge, A.; Wyder, S.; Huerta-Cepas, J.; Simonovic, M.; Doncheva, N.T.; Morris, J.H.; Bork, P.; et al. STRING v11: Protein-protein association networks with increased coverage, supporting functional discovery in genome-wide experimental datasets. *Nucleic Acids Res.* **2019**, *47*, D607–D613. [PubMed]
44. Oughtred, R.; Rust, J.; Chang, C.; Breitkreutz, B.; Stark, C.; Willems, A.; Boucher, L.; Leung, G.; Kolas, N.; Zhang, F.; et al. The BioGRID database: A comprehensive biomedical resource of curated protein, genetic, and chemical interactions. *Protein Sci.* **2021**, *30*, 187–200. [PubMed]
45. Orchard, S.; Ammari, M.; Aranda, B.; Breuza, L.; Briganti, L.; Broackes-Carter, F.; Campbell, N.H.; Chavali, G.; Chen, C.; Del-Toro, N.; et al. The MIntAct project--IntAct as a common curation platform for 11 molecular interaction databases. *Nucleic Acids Res.* **2014**, *42*, D358–D363. [PubMed]
46. Kanehisa, M.; Furumichi, M.; Tanabe, M.; Sato, Y.; Morishima, K. KEGG: New perspectives on genomes, pathways, diseases and drugs. *Nucleic Acids Res.* **2017**, *45*, D353–D361. [PubMed]
47. Fabregat, A.; Jupe, S.; Matthews, L.; Sidiropoulos, K.; Gillespie, M.; Garapati, P.; Haw, R.; Jassal, B.; Korninger, F.; May, B.; et al. The Reactome Pathway Knowledgebase. *Nucleic Acids Res.* **2018**, *46*, D649–D655. [PubMed]
48. Martens, M.; Ammar, A.; Riutta, A.; Waagmeester, A.; Slenter, N.; Hanspers, K.; Miller, R.A.; Digles, D.; Lopes, N.; Ehrhart, F.; et al. WikiPathways: Connecting communities. *Nucleic Acids Res.* **2021**, *49*, D613–D621. [PubMed]
49. Agrawal, A.; Balcı, H.; Hanspers, K.; Coort, S.L.; Martens, M.; Slenter, D.N.; Ehrhart, F.; Digles, D.; Waagmeester, A.; Wassink, I.; et al. WikiPathways 2024: Next generation pathway database. *Nucleic Acids Res.* **2024**, *52*, D679–D689. [PubMed]
50. Ma, L.; Zou, D.; Liu, L.; Shireen, H.; Abbasi, A.A.; Bateman, A.; Xiao, J.; Zhao, W.; Bao, Y.; Zhang, Z. Database Commons: A Catalog of Worldwide Biological Databases. *Genom. Proteom. Bioinform.* **2023**, *21*, 1054–1058. [CrossRef]
51. Blum, M.; Chang, H.-Y.; Chuguransky, S.; Grego, T.; Kandasaamy, S.; Mitchell, A.; Nuka, G.; Paysan-Lafosse, T.; Qureshi, M.; Raj, S.; et al. The InterPro protein families and domains database: 20 years on. *Nucleic Acids Res.* **2021**, *49*, D344–D354. [PubMed]
52. Hornbeck, P.V.; Zhang, B.; Murray, B.; Kornhauser, J.M.; Latham, V.; Skrzypek, E. PhosphoSitePlus, 2014: Mutations, PTMs and recalibrations. *Nucleic Acids Res.* **2015**, *43*, D512–D520. [PubMed]
53. Burley, S.K.; Bhikadiya, C.; Bi, C.; Bittrich, S.; Chao, H.; Chen, L.; Craig, P.A.; Crichlow, G.V.; Dalenberg, K.; Duarte, J.M.; et al. RCSB Protein Data bank: Tools for visualizing and understanding biological macromolecules in 3D. *Protein Sci.* **2022**, *31*, e4482. [CrossRef] [PubMed]
54. Thomas, P.D.; Ebert, D.; Muruganujan, A.; Mushayahama, T.; Albou, L.; Mi, H. PANTHER: Making genome-scale phylogenetics accessible to all. *Protein Sci.* **2022**, *31*, 8–22. [PubMed]
55. Peri, S.; Navarro, J.D.; Amanchy, R.; Kristiansen, T.Z.; Jonnalagadda, C.K.; Surendranath, V.; Niranjan, V.; Muthusamy, B.; Gandhi, T.; Gronborg, M.; et al. Development of human protein reference database as an initial platform for approaching systems biology in humans. *Genome Res.* **2003**, *13*, 2363–2371. [CrossRef] [PubMed]

56. Uhlen, M.; Zhang, C.; Lee, S.; Sjöstedt, E.; Fagerberg, L.; Bidkhori, G.; Benfeitas, R.; Arif, M.; Liu, Z.; Edfors, F.; et al. A pathology atlas of the human cancer transcriptome. *Science* **2017**, *357*, 2507. [CrossRef]
57. Knox, C.; Wilson, M.; Klinger, C.M.; Franklin, M.; Oler, E.; Wilson, A.; Pon, A.; Cox, J.; Chin, N.E.; Strawbridge, S.A.; et al. DrugBank 6.0: The DrugBank Knowledgebase for 2024. *Nucleic Acids Res.* **2024**, *52*, D1265–D1275. [PubMed]
58. Cannon, M.; Stevenson, J.; Stahl, K.; Basu, R.; Coffman, A.; Kiwala, S.; McMichael, J.F.; Kuzma, K.; Morrissey, D.; Cotto, K.; et al. DGIdb 5.0: Rebuilding the drug-gene interaction database for precision medicine and drug discovery platforms. *Nucleic Acids Res.* **2024**, *52*, D1227–D1235. [PubMed]
59. Treister, A.; Pico, A.R. Identifier Mapping in Cytoscape. *F1000Research* **2018**, *7*, 725. [CrossRef] [PubMed]
60. Otasek, D.; Morris, J.H.; Bouças, J.; Pico, A.R.; Demchak, B. Cytoscape Automation: Empowering workflow-based network analysis. *Genome Biol.* **2019**, *20*, 185. [CrossRef] [PubMed]
61. Doncheva, N.T.; Morris, J.H.; Holze, H.; Kirsch, R.; Nastou, K.C.; Cuesta-Astroz, Y.; Rattei, T.; Szklarczyk, D.; von Mering, C.; Jensen, L.J. Cytoscape stringApp 2.0: Analysis and Visualization of Heterogeneous Biological Networks. *J. Proteome Res.* **2023**, *22*, 637–646. [PubMed]
62. Gutierrez-Herrera, J.; Montero-Fernandez, M.A.; De Petris, L.; Guijarro, R.; Ekman, S.; Ortiz-Villalón, C. NTRK protein expression in NSCLC and its clinicopathological correlation. *Histol. Histopathol.* **2025**, *40*, 1569–1576. [PubMed]
63. Montero, M.A.; Aricak, O.; Kis, L.; Yoshikawa, A.; De Petris, L.; Grundberg, O.; Pham, H.H.; Roden, A.C.; Fukuoka, J.; Attanoos, R.; et al. Clinicopathological significance of the expression of PD-L1 in non-small cell lung cancer. *Ann. Diagn. Pathol.* **2021**, *51*, 151701. [CrossRef] [PubMed]
64. Gutierrez-Herrera, J.; Montero-Fernandez, M.A.; Kokaraki, G.; De Petris, L.; Maia Falcão, R.; Molina-Centelles, M.; Guijarro, R.; Ekman, S.; Ortiz-Villalón, C. NTRK Gene Expression in Non-Small-Cell Lung Cancer. *J. Respir.* **2025**, *5*, 2. [CrossRef]
65. Hermey, G. The Vps10p-domain receptor family. *Cell Mol. Life Sci.* **2009**, *66*, 2677–2689. [CrossRef] [PubMed]
66. Chen, S.; Crabill, G.A.; Pritchard, T.S.; McMiller, T.L.; Wei, P.; Pardoll, D.M.; Pan, F.; Topalian, S.L. Mechanisms regulating PD-L1 expression on tumor and immune cells. *J. Immunother. Cancer* **2019**, *7*, 305. [CrossRef] [PubMed]
67. Sharpe, A.H.; Pauken, K.E. The diverse functions of the PD1 inhibitory pathway. *Nat. Rev. Immunol.* **2018**, *18*, 153–167. [PubMed]
68. Benjamin, D.J.; Haslam, A.; Gill, J.; Prasad, V. Targeted therapy in lung cancer: Are we closing the gap in years of life lost? *Cancer Med.* **2022**, *11*, 3417–3424. [CrossRef] [PubMed]
69. Mountain, C.F. Revisions in the International System for Staging Lung Cancer. *Chest* **1997**, *111*, 1710–1717. [CrossRef] [PubMed]
70. Mamdani, H.; Matosevic, S.; Khalid, A.B.; Durm, G.; Jalal, S.I. Immunotherapy in Lung Cancer: Current Landscape and Future Directions. *Front. Immunol.* **2022**, *13*, 823618. [CrossRef] [PubMed]
71. Kalra, A.; Rashdan, S. The toxicity associated with combining immune check point inhibitors with tyrosine kinase inhibitors in patients with non-small cell lung cancer. *Front Oncol.* **2023**, *13*, 1158417. [CrossRef] [PubMed]
72. Wislet, S.; Vandervelden, G.; Rogister, B. From Neural Crest Development to Cancer and Vice Versa: How p75(NTR) and (Pro)neurotrophins Could Act on Cell Migration and Invasion? *Front. Mol. Neurosci.* **2018**, *11*, 244. [CrossRef]
73. Kaplan, D.R.; Miller, F.D. Neurotrophin signal transduction in the nervous system. *Curr. Opin. Neurobiol.* **2000**, *10*, 381–391. [CrossRef] [PubMed]
74. Topalian, S.L.; Drake, C.G.; Pardoll, D.M. Immune checkpoint blockade: A common denominator approach to cancer therapy. *Cancer Cell* **2015**, *27*, 450–461. [CrossRef] [PubMed]
75. Antonangeli, F.; Natalini, A.; Garassino, M.C.; Sica, A.; Santoni, A.; Di Rosa, F. Regulation of PD-L1 Expression by NF-κB in Cancer. *Front. Immunol.* **2020**, *11*, 584626. [CrossRef] [PubMed]
76. Yu, H.; Pardoll, D.; Jove, R. STATs in cancer inflammation and immunity: A leading role for STAT3. *Nat. Rev. Cancer* **2009**, *9*, 798–809. [CrossRef] [PubMed]
77. Konen, J.M.; Rodriguez, B.L.; Fradette, J.J.; Gibson, L.; Davis, D.; Minelli, R.; Peoples, M.D.; Kovacs, J.; Carugo, A.; Bristow, C.; et al. Ntrk1 Promotes Resistance to PD-1 Checkpoint Blockade in Mesenchymal Kras/p53 Mutant Lung Cancer. *Cancers* **2019**, *11*, 462. [CrossRef] [PubMed]
78. Ren, D.; Hua, Y.; Yu, B.; Ye, X.; He, Z.; Li, C.; Wang, J.; Mo, Y.; Wei, X.; Chen, Y.; et al. Predictive biomarkers and mechanisms underlying resistance to PD1/PD-L1 blockade cancer immunotherapy. *Mol. Cancer* **2020**, *19*, 19. [CrossRef] [PubMed]
79. Miranda, C.; Fumagalli, T.; Anania, M.C.; Vizioli, M.G.; Pagliardini, S.; Pierotti, M.A.; Greco, A. Role of STAT3 in in vitro transformation triggered by TRK oncogenes. *PLoS ONE* **2010**, *5*, e9446. [CrossRef] [PubMed]
80. Yu, H.; Boyle, T.A.; Zhou, C.; Rimm, D.L.; Hirsch, F.R. PD-L1 Expression in Lung Cancer. *J. Thorac. Oncol.* **2016**, *11*, 964–975. [CrossRef] [PubMed]
81. Chen, L.; Yang, F.; Feng, T.; Wu, S.; Li, K.; Pang, J.; Shi, X.; Liang, Z. PD-L1, Mismatch Repair Protein, and NTRK Immunohistochemical Expression in Cervical Small Cell Neuroendocrine Carcinoma. *Front. Oncol.* **2021**, *11*, 752453. [CrossRef] [PubMed]
82. Domagala-Kulawik, J. New Frontiers for Molecular Pathology. *Front. Med.* **2019**, *6*, 284. [CrossRef]
83. Dai, Y.; Liu, P.; He, W.; Yang, L.; Ni, Y.; Ma, X.; Du, F.; Song, C.; Liu, Y.; Sun, Y. Genomic Features of Solid Tumor Patients Harboring ALK/ROS1/NTRK Gene Fusions. *Front. Oncol.* **2022**, *12*, 813158. [CrossRef] [PubMed]

84. Schünemann, H.; Hill, S.; Guyatt, G.; Akl, E.A.; Ahmed, F. The GRADE approach and Bradford Hill's criteria for causation. *J. Epidemiol. Community Health* **2011**, *65*, 392–395. [PubMed]
85. Shimonovich, M.; Thomson, H.; Pearce, A.; Katikireddi, S.V. Applying Bradford Hill to assessing causality in systematic reviews: A transparent approach using process tracing. *Res. Synth. Methods* **2024**, *15*, 826–838. [CrossRef]
86. Salokas, K.; Liu, X.; Öhman, T.; Chowdhury, I.; Gawriyski, L.; Keskitalo, S.; Varjosalo, M. Physical and functional interactome atlas of human receptor tyrosine kinases. *EMBO Rep.* **2022**, *23*, e54041. [CrossRef] [PubMed]

Disclaimer/Publisher's Note: The statements, opinions and data contained in all publications are solely those of the individual author(s) and contributor(s) and not of MDPI and/or the editor(s). MDPI and/or the editor(s) disclaim responsibility for any injury to people or property resulting from any ideas, methods, instructions or products referred to in the content.